Inorganic Chemistry

Article

pubs.acs.org/IC

Redox and Photoinduced Electron-Transfer Properties in Short Distance Organoboryl Ferrocene-Subphthalocyanine Dyads

Eranda Maligaspe,[†] Matthew R. Hauwiller,[‡] Yuriy V. Zatsikha,[†,§] Jonathan A. Hinke,[‡] Pavlo V. Solntsev,[†,‡] David A. Blank,*[,‡] and Victor N. Nemykin*[,†]

[†]Department of Chemistry and Biochemistry, University of Minnesota Duluth, 1039 University Drive, Duluth, Minnesota 55812, United States

[‡]Department of Chemistry, University of Minnesota, 207 Pleasant Street SE, Minneapolis, Minnesota 55455, United States

[§]Institute of Organic Chemistry, National Academy of Sciences of Ukraine, 5 Murmanska str., 02660 Kyiv, Ukraine

Supporting Information

ABSTRACT: Reaction between ferrocene lithium or ethynylferrocene magnesium bromide and (chloro)-boronsubphthalocyanine leads to formation of ferrocene- (**2**) and ethynylferrocene- (**3**) containing subphthalocyanine dyads with a direct organometallic B−C bond. New donor−acceptor dyads were characterized using UV−vis and magnetic circular dichroism (MCD) spectroscopies, NMR method, and X-ray crystallography. Redox potentials of the rigid donor−acceptor dyads **2** and **3** were studied using the cyclic voltammetry (CV) and differential pulse voltammetry (DPV) approaches and compared to the parent subphthalocyanine **1** and conformationally flexible subphthalocyanine ferrocenenylmethoxide (**4**) and ferrocenyl carboxylate (**5**) dyads reported earlier. It was found that the first oxidation process in dyads **2** and **3** is ferrocene-centered, while the first reduction as well as the second oxidation are centered at the subphthalocyanine ligand. Density functional theory-polarized continuum model (DFT-PCM) and time-dependent (TD) DFT-PCM methods were used to probe the electronic structures and explain the UV−vis and MCD spectra of complexes **1**−**5**. DFT-PCM calculations suggest that the LUMO, LUMO+1, and HOMO-3 in new dyads **2** and **3** are centered at the subphthalocyanine ligand, while the HOMO to HOMO-2 in both dyads are predominantly ferrocene-centered. TDDFT-PCM calculations on compounds **1**−**5** are indicative of the $\pi \rightarrow \pi^*$ transitions dominance in their UV−vis spectra, which is consistent with the experimental data. The excited state dynamics of the parent subphthalocyanine **1** and dyads **2**−**5** were investigated using time-resolved transient spectroscopy. In the dyads **2**−**5**, the initially excited state is rapidly (<2 ps) quenched by electron transfer from the ferrocene ligand. The lifetime of the charge transfer state demonstrates a systematic dependence on the structure of the bridge between the subphthalocyanine and ferrocene.

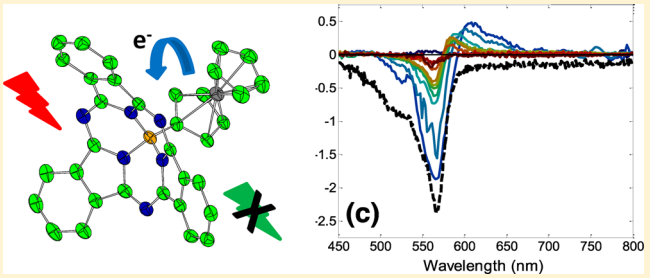

INTRODUCTION

Numerous donor−acceptor (D−A) dyads and donor−antennae−acceptor (D−An−A) triads were explored during the last several decades as prospective systems for artificial photosynthesis and solar energy conversion.[1−5] The electron transfer kinetics, the desired charge-separation (CS) state stability, and mechanism for the excited state relaxation dynamics in such D−A assemblies is influenced by the degree of electronic coupling between the donor and acceptor. Such coupling strongly depends on the distance between donor and acceptor, the donor−acceptor spatial orientation, and the electronic structure of the bridging group between them.[6] Other factors that could play a significant role in the formation and stability of CS state are intermolecular interactions and charge-recombination. It is commonly accepted that the donor−acceptor distance in corresponding dyad is the most important parameter for CS state formation and stability.[7] For instance, it has been shown that a short, ∼2.6 Å, distance in donor−acceptor dyad leads to formation of an exceptionally long-living (230 μs) CS state.[8]

Various porphyrins and their analogues were suggested as an effective antenna in donor−acceptor dyads. Among these, the subphthalocyanine (SubPc) macrocycle was intensively studied because of its specific absorption properties as well as nonplanar geometry. The bowl-shaped curvature of the SubPc may offer advantages for covalent and noncovalent coordination with nonplanar electron acceptors (i.e., carbon nanotubes and fullerenes).[9] SubPcs have higher fluorescence quantum yields and smaller reorganization energies than porphyrins.[10] Ferrocene-containing SubPcs reported by Torres and co-workers as well as our group have shown promising photophysical properties for applications in organic photovoltaics (OPV).[9,11] For instance, long-lived (up to 230 μs) CS

Received: June 18, 2014
Published: August 14, 2014

   dx.doi.org/10.1021/ic5014544 | *Inorg. Chem.* 2014, 53, 9336−9347

Scheme 1

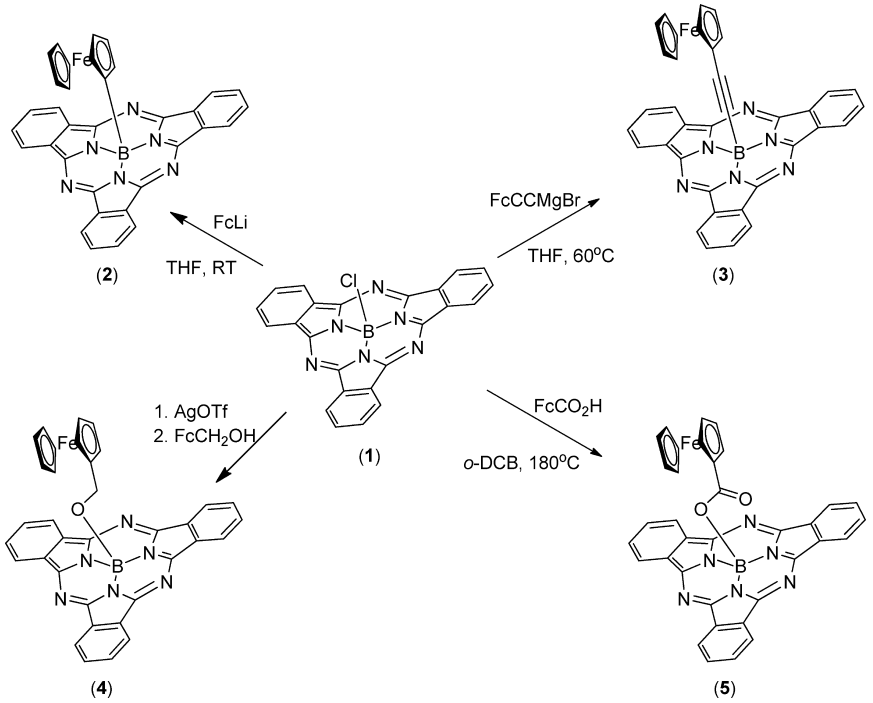

states were observed in D−A systems in which ferrocene substituents were axially connected via B−O bond (using a *p*-phenyloxy bridging group) to the SubPc.[9] Under the hypothesis that the shorter Fe-SubPc distance should increase the rate of CS state formation, we have recently prepared and characterized ferrocene SubPc dyads **4** and **5**. The ferrocene group in these dyads is connected to the central boron atom via carboxylic or alkoxide type covalent B−O bond (Scheme 1).[11] To our knowledge, more rigid Fc-SubPc dyads with a direct organoboron B−C bond have not been previously investigated. In this paper, we report synthesis, spectroscopic characterization, redox properties, and photophysics of two new Fc-SubPc donor−acceptor systems (Scheme 1) in which ferrocene (SubPcBFc, **2**) and ethynylferrocene (SubPcBC≡CFc, **3**) are bonded to the central boron atom of the SubPc macrocycle via B−C bond. The redox and photophysical properties of these new dyads are compared to those in dyads **4** and **5** as well as the parent SubPcBCl **1** (Scheme 1).

EXPERIMENTAL SECTION

Reagents and Materials. All reactions were performed under an argon atmosphere using standard Schlenk techniques. Solvents were purified using standard approaches: toluene was dried over sodium metal, THF was dried over sodium-potassium alloy, and hexane and DCM were dried over calcium hydride. SubPcBCl (**1**), ethynylferrocene, and ethylmagnesium bromide were purchased from Aldrich and used without further purification. Bromoferrocene was purchased from Alfa Aesar. SubPcBOCH$_2$Fc (**4**) and SubPcBO$_2$CFc (**5**) were prepared as described earlier.[11] Silica gel (60 Å, 60−100 μm) was purchased from Dynamic Adsorbents Inc.

Preparation of SubPcBFc (2). Bromoferrocene (258 mg, 0.975 mmol) was dissolved in anhydrous THF (7 mL) under Ar purge. After 5 min, BuLi (0.371 mL, 2.5 M in THF) was added to the bromoferrocene solution and stirred at −78 °C for 15−20 min. The orange color reaction mixture was then allowed to warm to ambient temperature. After this procedure, the ferrocene lithiated solution was transferred into a solution of SubPcBCl (100 mg, 0.232 mmol), and the resulting solution was stirred for 2 h (complete consumption of the SubPcBCl was observed by TLC). The solvent was evaporated under reduced pressure. Column chromatography on neutral alumina with hexane/CH_2Cl_2 (40:60, v/v) as eluent gave the titled compound. Yield 28.2 mg (21%). Elemental analysis: calculated for $C_{34}H_{21}BN_6Fe$ x $0.5CH_2Cl_2$ x $1.3C_6H_{14}$: C, 69.15; H, 5.51; N, 11.44. Found: C, 69.05; H, 5.19; N, 11.46. ^{1}H NMR [500 MHz, δ, ppm, $CDCl_3$]: 8.85 (6H, dd, J = 5.80 Hz, J = 2.90 Hz, α-SubPc), 7.90 (6H, dd, J = 5.80, J = 2.90, β-SubPc), 3.56 (5H, s, Cp), 3.50 (2H, m, J = 1.67 Hz, β-Cp), 2.38 (2H, m, J = 1.67 Hz, α-Cp). ^{13}C NMR [125 MHz, δ, ppm, $CDCl_3$]: 150.9 (α-pyrrole), 130.9 (β-pyrrole), 129.6 (α-SubPc), 122.1 (β-SubPc), 77.3 (C_{ipso}), 68.6 (α-Cp), 68.4 (β-C_p), 67.8 (C_p).

Preparation of SubPcBCCFc (3). Ethylmagnesium bromide (0.240 mL, 0.719 mmol, 3 M in ether) was added to a solution of ethynylferrocene (170 mg, 0.812 mmol) in anhydrous THF (5 mL). The resulting mixture was refluxed at 60 °C for 1.5 h and cooled down to room temperature. The ferrocenyl Grignard mixture was then transferred via canula to a solution of SuPcBCl (100 mg, 0.232 mmol) in anhydrous THF (15 mL). The mixture was stirred at room temperature for 1 h (complete consumption of the SubPcBCl was observed by TLC). The solvent was evaporated, and the crude product was subjected to a neutral alumina column to obtain the desired product using hexane/CH_2Cl_2 = 20:80 v/v as eluent. Yield: 36.4 mg, 26%. Elemental analysis: calculated for $C_{36}H_{21}BN_6Fe$ x $0.4CH_2Cl_2$ x $0.6C_6H_{14}$: C, 69.63; H, 4.41; N, 12.18. Found: C, 69.94; H, 3.73; N, 12.32. ^{1}H NMR [500 MHz, δ, ppm, $CDCl_3$]: 8.82 (6H, dd, J = 5.90 Hz, J = 2.94 Hz, α-SubPc), 7.82 (6H, dd, J = 5.90 Hz, J = 2.94 Hz, β-SubPc), 3.82 (2H, m, J = 1.80 Hz, β-Cp), 3.79 (5H, s, Cp), 3.78 (2H, m, J = 1.80 Hz, α-Cp). ^{13}C NMR [125 MHz, δ, ppm, $CDCl_3$]: 150.5 (α-pyrrole), 130.9 (β-pyrrole), 129.7 (α-SubPc), 122.2 (β-SubPc), 93.2 (-C≡C−), 77.3 (Cipso), 71.2 (α-Cp), 69.8 (Cp), 68.2 (β-Cp), 64.6 (-C≡C−).

DFT-PCM and TDDFT-PCM Calculations. The starting geometries of compounds **1**−**5** were adopted from the experimental X-ray data and were optimized using a hybrid PBE1PBE exchange-correlation functional.[12] This PBE1PBE exchange-correlation functional was found to result in good agreement between calculated and experimentally determined bond distances and angles in ferrocene-containing compounds.[13] Energy minima in optimized geometries were confirmed by the frequency calculations (absence of the imaginary frequencies). Solvent effects were calculated using the

dx.doi.org/10.1021/ic5014544 | Inorg. Chem. 2014, 53, 9336−9347

polarized continuum model (PCM).[14] In all calculations, DCM was used as the solvent. A pure BP86 exchange-correlation functional was used in all single-point DFT-PCM and TDDFT-PCM calculations,[15] because it is more accurate in calculations of the vertical excitation energies in a variety of porphyrins and their analogues.[16] In all PCM-TDDFT calculations, the first 50 states were calculated. In all calculations, full-electron Wachter's basis set[17] was utilized for iron atoms, while all other atoms were modeled using the 6-31G(d)[18] basis set. Gaussian 09 software was used in all calculations.[19] QMForge program was used for molecular orbital analysis.[20]

X-ray Crystallography. Useful for X-ray crystallographic experiments single crystals of dyads **2** and **3** were prepared by the slow evaporation of saturated DCM/hexane solutions. A Rigaku RAPID-II diffractometer with a graphite monochromator and Mo Kα (λ = 0.71073 Å) radiation was used for X-ray diffraction data collection. All experiments were conducted at −150 °C temperature. Multiscan absorption correction[21] was applied to the data in all cases. The crystal structures were solved by the direct method (SIR-92)[22] and refined by full-matrix least-squares method based on F^2 using the SHELXL-2013 and SHELXLE programs.[23] All non-hydrogen atoms were refined anisotropicaly, while hydrogen atoms were refined using "riding mode" with displacement parameters bonded to a parent atom: $U_{iso}(H) = 1.2U_{eq}(C)$ ($U_{eq} = 1/3(U_{11} + U_{22} + U_{33})$).

The ethynylferrocene group in **3** was found to be disordered over two positions by an rotation along the C−B bond by an angle (Supporting Information, Figure S1). The final refined occupancies were found to be 0.61 and 0.39, respectively. A standard set of geometrical restraints such as DELU and SIMU was used during the refinement. Also, in solvent DCM molecule one chloride atom was found to be disordered over two positions with occupancies 0.56 and 0.44, respectively. The structure also contains voids of volume 182 Å^3 that occupied by a disordered solvent. Unfortunately, we were not able to find a good model for disordered molecules, and the SQUEEZE routine implemented in PLATON was used to remove a contribution of the disordered part from the overall diffraction data. The analyses of the structures and visualization of the results were done using PLATON software. Crystal data for complexes **2** and **3** are summarized in Table 1, while selected bond distances and angles are presented in Table 2. CCDC 1008499 and 1008500 contain the supplementary crystallographic data for all compounds. These data can be obtained free of charge via www.ccdc.cam.ac.uk/conts/retrieving.html (or from Cambridge Crystallographic Data Centre, 12 Union Road, Cambridge CB2 1EZ, UK; fax: (+44) 1223-336-033 or deposit@ccdc.cam.ac.uk).

Spectroscopy Measurements. Jasco-720 spectrophotometer was used to collect UV−vis data. OLIS DCM 17 CD spectropolarimeter with a 1.4 T DeSa magnet was used to collect MCD data. The MCD spectra were measured in mdeg = [θ] and converted to $\Delta\varepsilon$ (M^{-1} cm^{-1} T^{-1}) using the regular conversion formula: $\Delta\varepsilon = \theta/(32980 \cdot Bdc)$, where B is the magnetic field, d is the path length, and c is the concentration. Complete spectra were recorded at room temperature in parallel and antiparallel directions with respect to the magnetic field. Electrochemical measurements were conducted using a CH Instruments electrochemical analyzer utilizing a three-electrode scheme with platinum working, auxiliary and Ag/AgCl reference electrodes. DCM or DMF were used as solvents and 0.1 M solution of tetrabutylammonium perchlorate (TBAP) was used as electrolyte. In all cases, experimental redox potentials were corrected using decamethylferrocene (Fc*H) as an internal standard. NMR spectra were recorded on a Varian INOVA instrument with a 500 MHz frequency for protons and 125 MHz for carbon. Chemical shifts are reported in parts per million (ppm) and referenced to tetramethylsilane ($Si(CH_3)_4$) as an internal standard. In all cases, final assignments of ^{1}H and ^{13}C signals were made using COSY and HMQC spectra. Elemental analyses were conducted by Atlantic Microlab. Steady-state fluorescence data were collected using a Cary Eclipse fluorimeter at room temperature.

Fluorescence lifetimes were measured using time correlated single photon counting. Samples in a 1 cm quartz cuvette were excited with a 472 nm, 40 MHz diode laser (Driver: Picoquant PDL 800-B; Head: Picoquant LDH-P-470). Emission was directed through a double monochromator (Jobin-Yvon DH-10) and detected using an avalanche photodiode (Picoquant MPD PDM). The instrument response of the system is approximately 500 ps fwhm.

Pump−probe spectroscopy allowed for the time-resolved measurement of nonemissive samples. A home-built laser system consisting of a Ti:sapphire oscillator (powered by a Spectra Physics Millenia Pro) and regenerative amplifier (powered by a Spectra Physics Empower 15) generated ∼60 fs (fwhm), 0.8 mJ, 805 nm pulses at a repetition rate of 1 kHz. A portion of this light was directed into a home-built noncollinear optical parametric amplifier (NOPA) to create excitation pulses at 560 nm. Continuum probe pulses (420−750 nm) were created by focusing a small fraction of the 805 nm light (∼20 μW) into a 2 mm sapphire window. The excitation light was polarized at 54.7 deg relative to the probe polarization (the magic angle) to isolate the isotropic dynamics of the excited state. Time delay between the excitation and probe pulses was controlled by a mechanical delay stage (Newport UTM150PP.1). After the pulses were focused in the sample, the probe beam was collimated, directed through a monochromator (Princeton Instruments SP2150i), and detected using a 256 pixel diode array (Hamamatsu S3902-256Q) giving a resolution of ∼2 nm per pixel. The pump beam was modulated at half the laser repetition rate, while the probe beam was measured for every laser pulse allowing for the change in optical density, ΔOD, induced by the pump to be calculated for each pulse pair. The dependence of the ΔOD signal for pulse energies between 10 and 40 nJ was found to be linear. Data shown were collected with pulse energies of 25−35 nJ. Samples had an optical density of 0.25 at the excitation wavelength and were continuously pumped through a 1 mm flow cell during data collection to ensure a fresh sample for each laser pulse. Absorption spectra taken before and after the pump probe experiments were indistinguishable, indicating no evidence of sample degradation.

RESULTS AND DISCUSSION

Synthesis. The direct attachment of ferrocene to the SubPcBCl (compound **2**) was achieved by the room-temperature reaction between the parent compound **1** and ferrocenyllithium salt prepared from BuLi and bromoferrocene in THF at −78 °C.[24] The synthetic route for compound (**3**) includes the

Table 1. Summary of Crystallographic Data for Compounds 2 and 3

	2	3
empirical formula	$C_{34}H_{21}BFeN_6$	$C_{36.25}H_{21.5}BCl_{0.5}FeN_6$
formula weight	580.23	625.48
crystal system	triclinic	triclinic
space group, Z	$P\bar{1}$, 2	$P\bar{1}$, 4
a (Å)	10.0410(4)	13.2281(8)
b (Å)	11.8991(5)	13.6458(9)
c (Å)	12.3514(8)	19.1772(14)
α (deg)	102.901(7)	71.365(5)
β (deg)	105.917(8)	89.078(6)
γ (deg)	107.811(8)	71.701(5)
volume (Å^3)	1272.8(1)	3100.6(4)
ρ_{calc}(g/cm^3)	1.514	1.340
μ(Mo K$_\alpha$) (mm^{-1})	0.631	0.566
θ_{max} (deg)	27.482	24.712
R_{int}	0.0388	0.0711
GOF (F^2)	1.100	1.055
$R_1{}^a$ ($F^2 > 2\sigma(F^2)$)	0.0466	0.0863
$wR_2{}^b$ (all data)	0.1432	0.2696
$\Delta\rho_{max}/\Delta\rho_{min}$ (e/Å^3)	0.618/−0.799	0.908/−1.012

$^aR_1(F) = \sum||F_o| - |F_c||/\sum|F_o|$. $^bwR_2(F^2) = \{\sum[w(F_o^2 - F_c^2)^2]/\sum w(F_o^2)^2]\}^{1/2}$.

dx.doi.org/10.1021/ic5014544 | Inorg. Chem. 2014, 53, 9336−9347

Table 2. Selected Bond Lengths (Å) and Angles (deg) for Compounds 2−3

Compound **2**			
N(1)−B(1)	1.505(4)	N(5)−B(1)−C(25)	114.9(2)
N(3)−B(1)	1.512(4)	N(1)−B(1)−C(25)	117.6(2)
N(5)−B(1)	1.502(4)	N(3)−B(1)−C(25)	114.5(2)
C(25)−B(1)	1.582(4)	N(5)−B(1)−N(3)	102.3(2)
N(5)−B(1)−N(1)	102.8(2)	N(1)−B(1)−N(3)	102.8(2)
Fe−C (average)	2.047(3)	Fe···π^a	1.648(2), 1.656(2)
Compound **3**			
N(1)−B(1)	1.502(7)	N(7)−B(2)	1.486(9)
N(3)−B(1)	1.492(7)	N(9)−B(2)	1.485(9)
N(5)−B(1)	1.504(8)	N(11)−B(2)	1.513(8)
C(25)−B(1)	1.583(9)	C(61A)−C(62A)	1.163(13)
B(2)−C(61A)	1.617(13)	C(62A)−C(63A)	1.368(15)
N(3)−B(1)−N(1)	102.5(4)	N(1)−B(1)−N(5)	103.3(5)
N(3)−B(1)−N(5)	102.6(4)	N(3)−B(1)−C(25)	115.7(5)
N(1)−B(1)−C(25)	116.5(4)	N(5)−B(1)−C(25)	114.3(4)
N(9)−B(2)−N(7)	103.6(5)	N(9)−B(2)−N(11)	104.0(5)
N(7)−B(2)−N(11)	103.9(6)	N(9)−B(2)−C(61A)	121.7(8)
N(7)−B(2)−C(61A)	110.7(7)	N(11)−B(2)−C(61A)	111.2(8)
Fe−C (average)	2.029(8)	Fe···π^a	1.662(5), 1.637(7), 1.644(3), 1.644(4)

[a]The centroids were defined for each cyclopentadienyl ring of the ferrocenyl moieties.

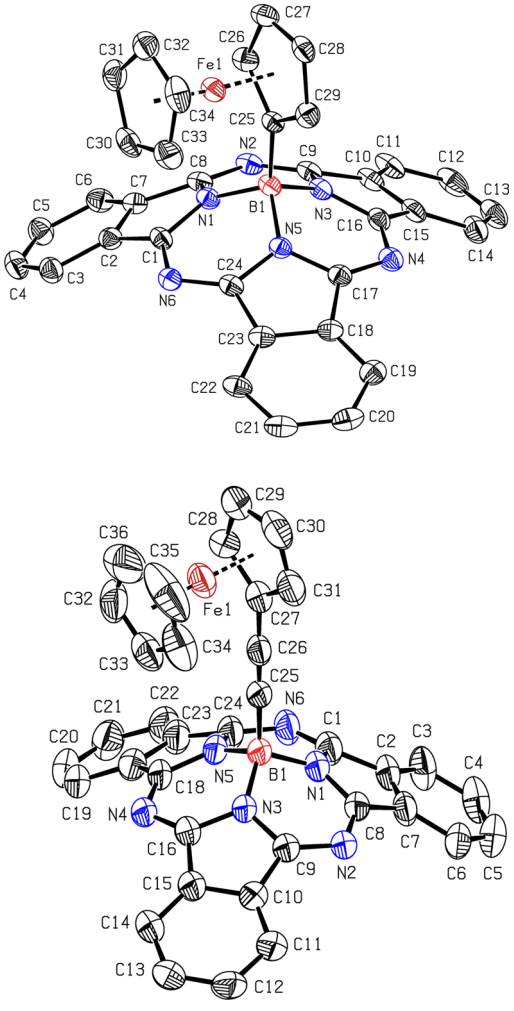

Figure 1. Labeled ORTEP diagram for X-ray structures of **2** (top) and **3** (bottom, only nondisordered unique molecule is shown). Hydrogen atoms are omitted for clarity. The thermal ellipsoid probability level is 50%.

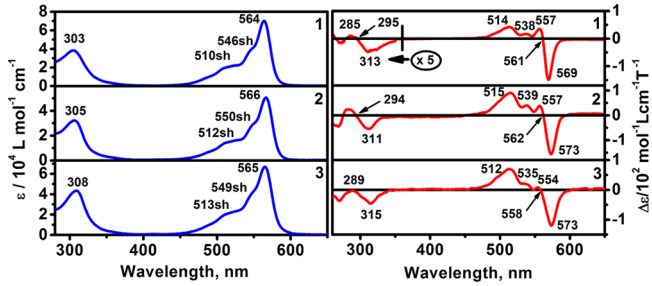

Figure 2. UV−vis (left) and MCD (right) spectra of compounds **1**−**3**.

Table 3. UV-vis Spectra and Time Constants Data for Compounds 1−5

	UV−vis	transient absorption time constants[a]	
compound	λ, nm ($\varepsilon/10^4$)	τ_{ET}, ps	τ_{BET}, ps
1	564 (7.01), 546sh, 510sh, 303 (3.83)		
2	566 (5.06), 550sh, 512sh, 305 (3.21)	0.2 ± 0.1	41 ± 1
3	565 (6.69), 549sh, 513sh, 308 (4.34)	1.9 ± 0.1	80 ± 4
4	562 (10.96), 543sh, 520sh, 306 (5.37)	5.1 ± 0.1	350 ± 10
5	564 (11.75), 546sh, 508sh, 302 (6.92)	1.5 ± 0.1	224 ± 4

[a]τ_{ET} is a time constant for the initial electron transfer, and τ_{BET} is a time constant for the subsequent back electron transfer (see Discussion for details).

axial chlorine atom substitution in the starting SubPcBCl (**1**) with the ethynylferrocene-Grignard reagent prepared from ethynylferrocene and ethyl magnesium bromide in hot THF.[25] Both compounds are surprisingly stable at ambient conditions and were purified by chromatography method using neutral alumina. The relatively low yields of the target products **2** and **3** (21−26%) could be attributed to the well-known low stability of subphthalocyanine core in basic conditions.[9] The ethynyl linker in compound **3** promotes stereochemical rigidity and potentially better through bonds electron-transfer properties

dx.doi.org/10.1021/ic5014544 | Inorg. Chem. 2014, 53, 9336−9347

Table 4. Redox Potentials of Compounds 1−5 (DCM/0.1M TBAP)

	oxidation, V		reduction, V
	E^{Ox2}	$E_{1/2}^{Ox1}$ (Fc)	$E_{1/2}^{R1}$
1[b,c]	0.655[a]		−1.698[a]
2	0.754[a]	0.050	−1.579
3	0.546[a]	0.089	−1.550
3[b]	0.57[a]	0.120	−1.398
4[b,c]	0.545[a]	0.020	−1.505
5[b,c]	0.725[a]	0.345	−1.323

[a]Irreversible process; all potentials (±5 mV) are given in volts relative to FcH/FcH$^+$. [b]Data for DMF/TBAP system. [c]From ref 11.

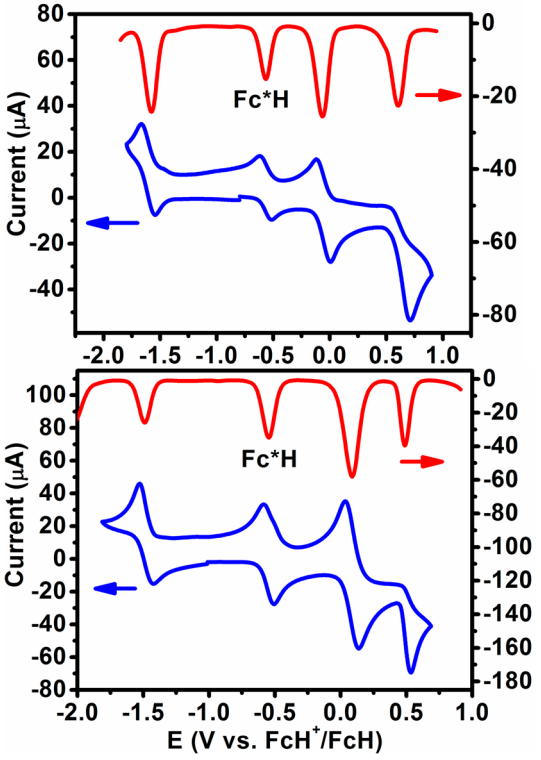

Figure 3. Room-temperature CV (100 mV/s, blue) and DPV (red) data for compounds **2** (top) and **3** (bottom) in DCM/0.1 M TBAP system (Fc*H is decamethylferrocene used as internal standard).

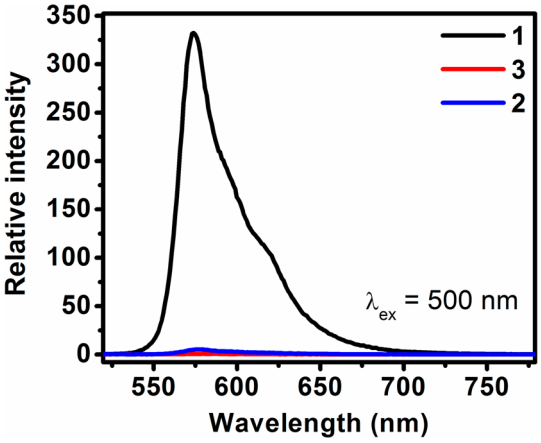

Figure 4. Relative fluorescence spectra of compounds **1** (black), **2** (blue), and **3** (red) following excitation at 500 nm in DCM.

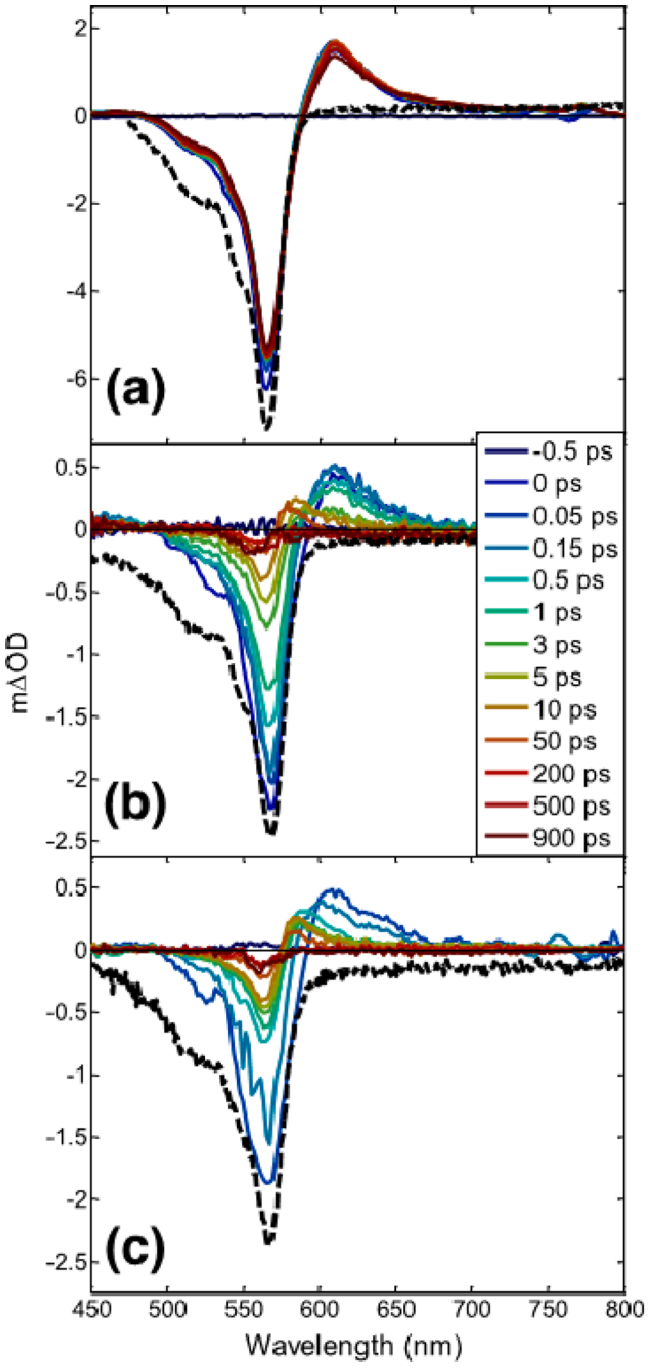

Figure 5. Transient spectra following excitation at 560 nm for (a) **1**, (b) **3**, and (c) **2**. The dashed lines are the inverted absorption spectra for reference.

than B−O linker in the dyads **4** and **5** which we discussed in our previous publication.[11] To the best of our knowledge, the dyads **2** and **3** are the first reported subphthalocyanine-ferrocene compounds containing the B−C bond. Moreover, structural rigidity and very short B−Fe distances, which are present in dyads **2** and **3**, suit these complexes for potentially fast photoinduced electron transfer processes.[9]

X-ray Crystal Structures. A decisive confirmation on the chemical structures of ferrocenyl-subphthalocyanine complexes **2** and **3** was obtained from the single-crystal X-ray data. Refinement parameters for compounds **2** and **3** are shown in Table 1, while important bonds lengths and bond angles are

dx.doi.org/10.1021/ic5014544 | Inorg. Chem. 2014, 53, 9336−9347

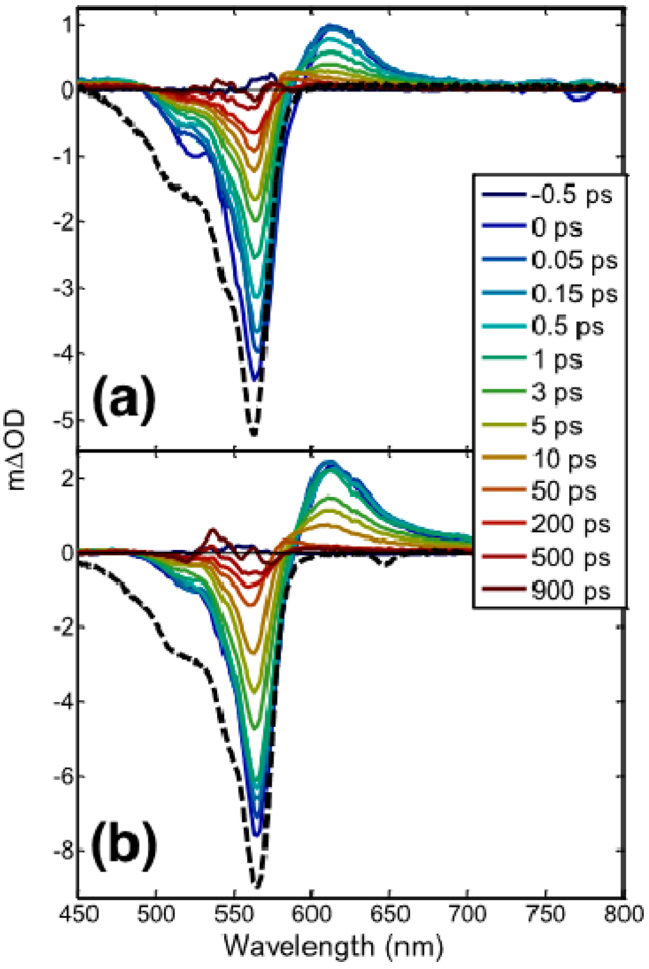

Figure 6. Transient spectra following excitation at 560 nm for (a) **4** and (b) **5**. The dashed lines are the inverted absorption spectra for reference.

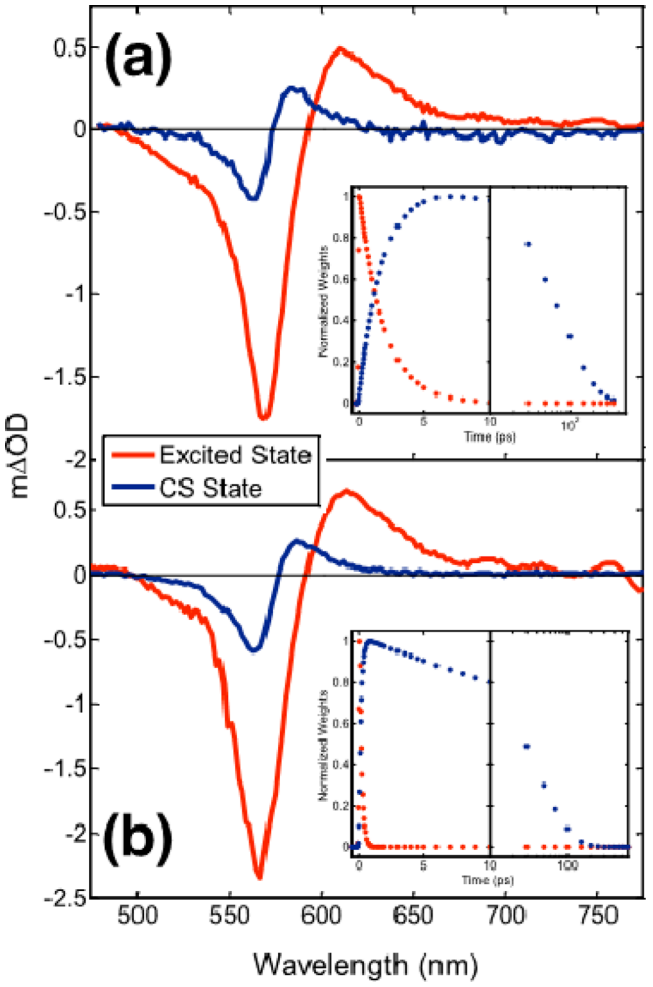

Figure 7. Two primary spectral components used to fit the time-dependent spectra shown in Figure 5b,c for (a) **3** and (b) **2**. The insets show the weights of the two fitting components as a function of time. Direct comparisons of the total fits to the raw data at selected time delays are provided in the Supporting Information.

listed in Table 2. ORTEP drawings of compounds **2** and **3** are presented in Figure 1. In agreement with all previously reported structures of SubPc compounds,[9,26−29] the subphthalocyanine core reveal a bowl-shaped nonplanar conformation with the boron atom positioned above the plane formed by the isoindole nitrogen atoms. In both dyads **2** and **3**, the boron center is present in a trigonal pyramidal (3N+C) coordination. The axial B−C bond in **2** and **3** are virtually the same (1.582(4) and 1.583(9)Å, respectively) and compatible with previously reported C-substituted subphthalocyanines.[27,30] Equatorial B−N bonds in complexes **2** and **3** are very similar but slightly longer than B−N bonds in the macrocycle **1** and dyads **4** and **5**.[11] The C≡C bond in dyad **3** is quite short (1.163(13) Å) and comparable with the bond in $(Bu)_2$N-(*p*-Ph)-C≡C-BSubPc.[30] At the same time less rich phenyl group tends to contract the C≡C bond and thus in case of *p*-tolyl substituent the same bond is longer (1.192(4) Å). The Fe−C bond distances were found to be in the typical for ferrocene derivatives range (Table 2). The Cp rings in dyads **2** and **3** were found to be in conformation close to an eclipse. The B−Fe distance in **2** (3.337(4) Å) is the shortest among all known ferrocene-subphthalocyanine dyads, and it is obviously longer in dyad **3** (5.629(3)−5.640(7) Å). The packing diagram for complexes **2** and **3** is shown in Supporting Information, Figure S2 and indicative of intermolecular $\pi-\pi$ stacking between nearby isoindole rings of the SubPc ligand.

Spectroscopy. Because of the presence of the ferrocene groups in dyads **2** and **3**, their solubility in common organic solvents is much higher as compared to the unsubstiuted macrocycle **1**. For instance, donor−acceptor dyads **2** and **3** are quite soluble in DCM, DMF, toluene, THF, and chloroform. ^{1}H NMR spectroscopy on dyads **2** and **3** confirms the axial chloride substitution in SubPcBCl **1** by the ferrocene and the ethynylferrocene. Indeed, signals of protons of the Cp ligands in complexes **2** and **3** are shifted to higher fields in comparison with the respecting signals in the parent FcH and FcC≡CH molecules, and such behavior is very characteristic for the axially coordinated phthalocyanines and their analogues[31] (Supporting Information, Figures S3 and S4). Because of the shorter distance between ferrocene group and the macrocycle, α-Cp and β-Cp proton signals in dyad **2** were observed at 2.37 and 3.50 ppm, while those in dyad **3** were detected at 3.785 and 3.82 ppm, respectively. NMR chemical shifts for the subphthalocyanine protons in dyads **2** and **3** are very similar, which is indicative of a negligible effect of the axial group on the NMR chemical shifts. A close behavior was found in the other axially substituted SubPcs.[9,26−30]

UV−vis and MCD spectra of SubPcs **1**−**3** are shown in Figure 2, and their numeric values are listed in Table 3. Similar

dx.doi.org/10.1021/ic5014544 | *Inorg. Chem.* 2014, 53, 9336−9347

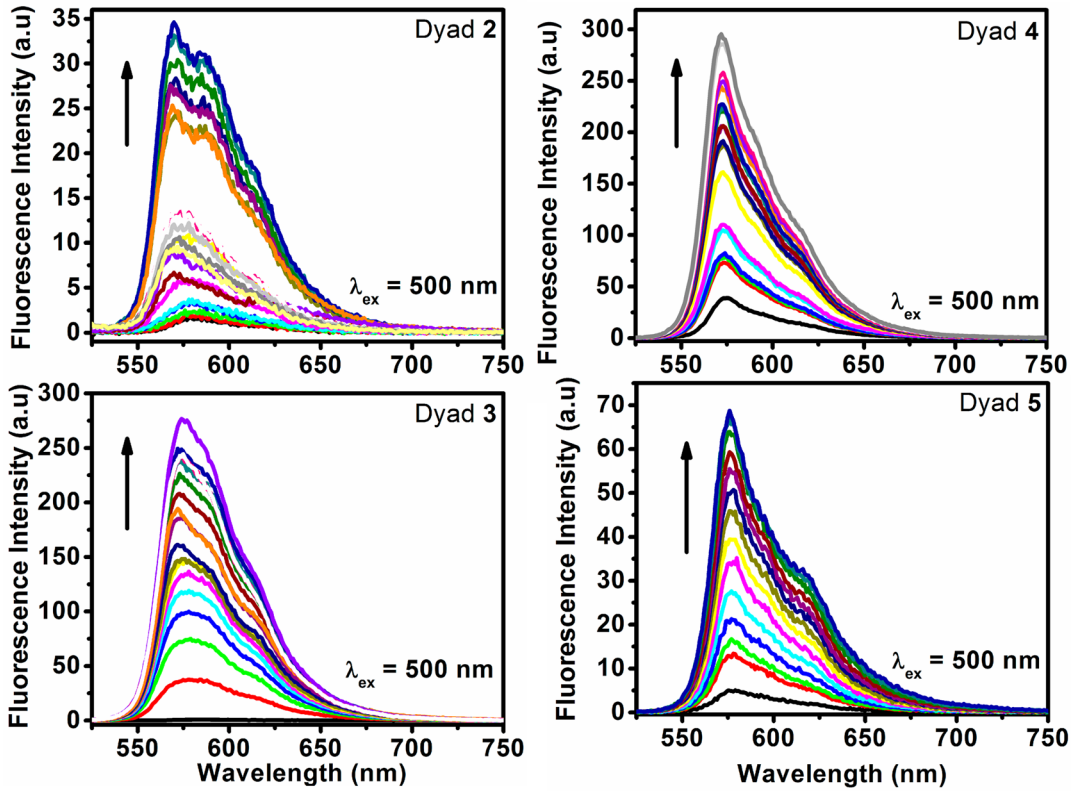

Figure 8. Fluorescence spectra change upon oxidation of dyads **2**–**4** with $Fe(ClO_4)_3$ and dyad **5** with Br_2 in DCM.

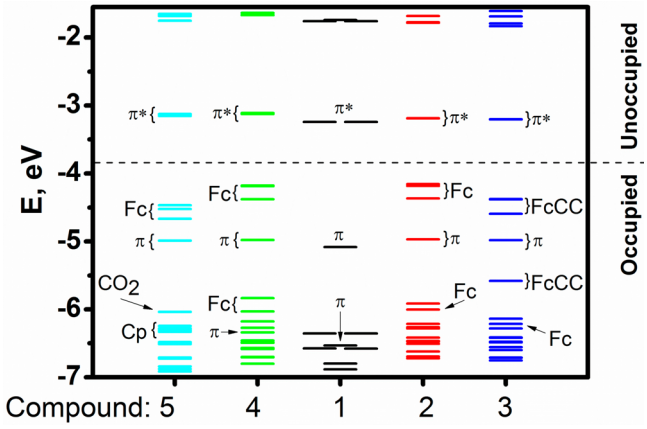

Figure 9. MO energy diagram for compounds **1**–**5** predicted at the DFT-PCM level.

to the previous reports on SubPcs,[9,11,26−32] replacement of the chlorine atom by ferrocene or ethynylferrocene groups in dyads **2** and **3** has a minimal influence on their UV−vis and MCD spectra, which consist of the intense SubPc centered $\pi \rightarrow \pi^*$ transitions. For instance, an intense low-energy Q-band is found at 565 nm in dyad **3**, which differs by only 1 nm from parent **1**, while only a 2 nm red-shift for the Q-band is found for dyad **2**. Not surprisingly, the MCD spectra of dyads **2** and **3** are very close to each other as well as to the MCD spectrum of initial subphthalocyanine **1**. Indeed, the most prominent feature in the MCD spectra of dyads **2** and **3** is the MCD Faraday A-term observed at 562 nm (dyad **2**) and 558 nm (dyad **3**), which correlates well with the most intense Q-band band observed in the UV−vis spectra of complexes **2** and **3**. The presence of this MCD Faraday A-term also confirms 3-fold effective symmetry in these dyads. As it will be concluded below, electrochemical data and theoretical modeling are indicative of ferrocene-centered HOMO to HOMO-2 MOs in complexes **2** and **3**. Such an electronic structure could result in observable low-energy metal-to-ligand charge-transfer (MLCT) transitions in the NIR region for complexes **2** and **3**. Although we tested the presence of such MLCT transitions in UV−vis spectra of dyads **2** and **3**, no evidence for such transitions was found.

Redox properties of the ferrocene-subphthalocyanine dyads were examined using cyclic voltammetry (CV) and differential pulse voltammetry (DPV) approaches (Table 4 and Figure 3). In order to compare redox properties of new dyads **2** and **3** with redox potentials of the earlier reported dyads **4** and **5**[11] as well as parent subphthalocyanine **1**, we first conducted electrochemical experiments in a DMF/0.1 M TBAP system. Dyad **2**, however, showed low stability in this system, and thus the only reliable data were collected for complex **3** (Table 4). Fortunately, both dyads **2** and **3** were found to be stable in less polar DCM solvent, and thus separate set of electrochemical experiments was conducted in the DCM/0.1 M TBAP system. In general, electrochemical data on dyads **2** and **3** are consistent with previously reported redox properties of complexes **4** and **5**. Specifically, the first oxidation and reduction processes were found to be reversible, while the second oxidation is a irreversible process (Figure 3). The axial ferrocene group oxidation in complex **2** was found at ∼40 mV lower potential as compared to ferrocene group oxidation in complex **3**, and this observation is in a good agreement with stronger electron-donating properties of the ferrocene group in dyad **2** compared to electron-donating properties of ethynylferrocene group in complex **3**. Similarly, the first, subphthalocyanine-based, reduction in complex **2** observed at ∼30 mV more negative potential compared to the same process in **3**. Second oxidation

dx.doi.org/10.1021/ic5014544 | Inorg. Chem. 2014, 53, 9336−9347

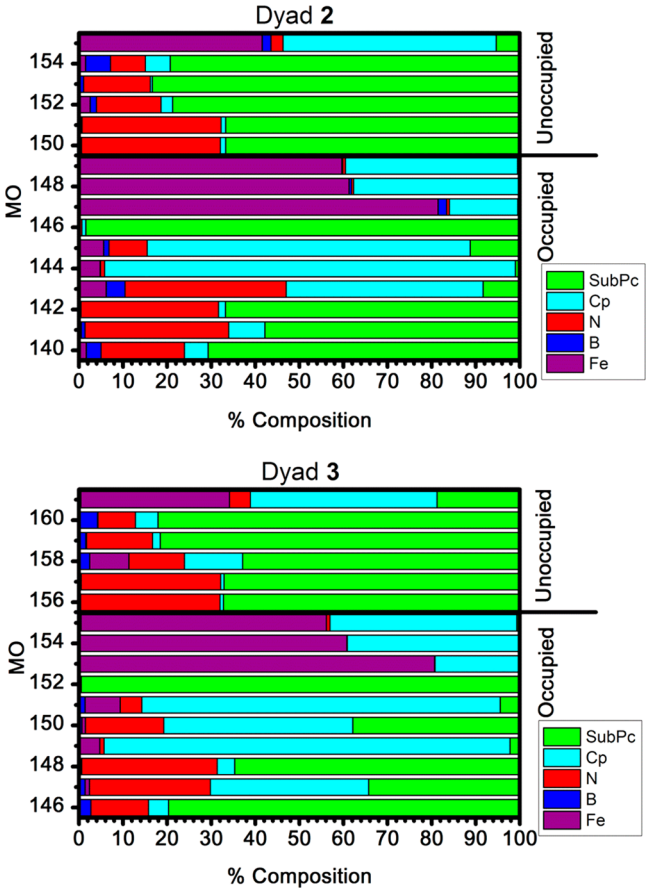

Figure 10. Molecular orbital compositions of compounds **2** and **3** predicted at the DFT-PCM level.

process was assigned to the oxidation of the subphthalocyanine core. This process was found to be the only partially reversible because of the significant degradation of the subphthalocyanine core, which is in excellent agreement with the earlier publications.[9,26−28,33]

Axially substituted SubPcs have well-documented fluorescent properties and able to participate in energy and/or electron transfer processes.[9−11] The parent SubPcBCl **1** has a high fluorescence quantum yield (Φ_F = 0.33, in agreement with the previous report[11]). Such a high quantum yield provides an easily accessible indication of excited-state deactivation in the dyads. For instance, upon the excitation at Q-band wavelength, the initial macrocycle **1** exhibits a very strong emission observed at 581 nm, which is assigned to the $S_1 \leftarrow S_0$ transition of the SubPc core (Figure 4). The fluorescence observed in SubPcs has been shown to be the mirror image of the Q-band absorption, has a small Stokes shift, and has only small dependence on the solvent polarity and the type of the axial group. Upon recording of the fluorescence spectra of complexes **1**−**5** at the same experimental concentration, excitation wavelength, intensity, and resolution, it was found that the emission intensities in dyads **2**−**5** are only 1%−3% of the emission from **1**. In addition, the weak emission from the dyads was spectrally indistinguishable from **1**, suggesting that the measured emission was coming from small amounts of residual precursor, **1**, or its hydroxide analogue (Supporting Information, Table S1). Efficient emission quenching was previously reported in several SubPcs with different quenching groups.[9−11] Here we employed pump−probe spectroscopy to

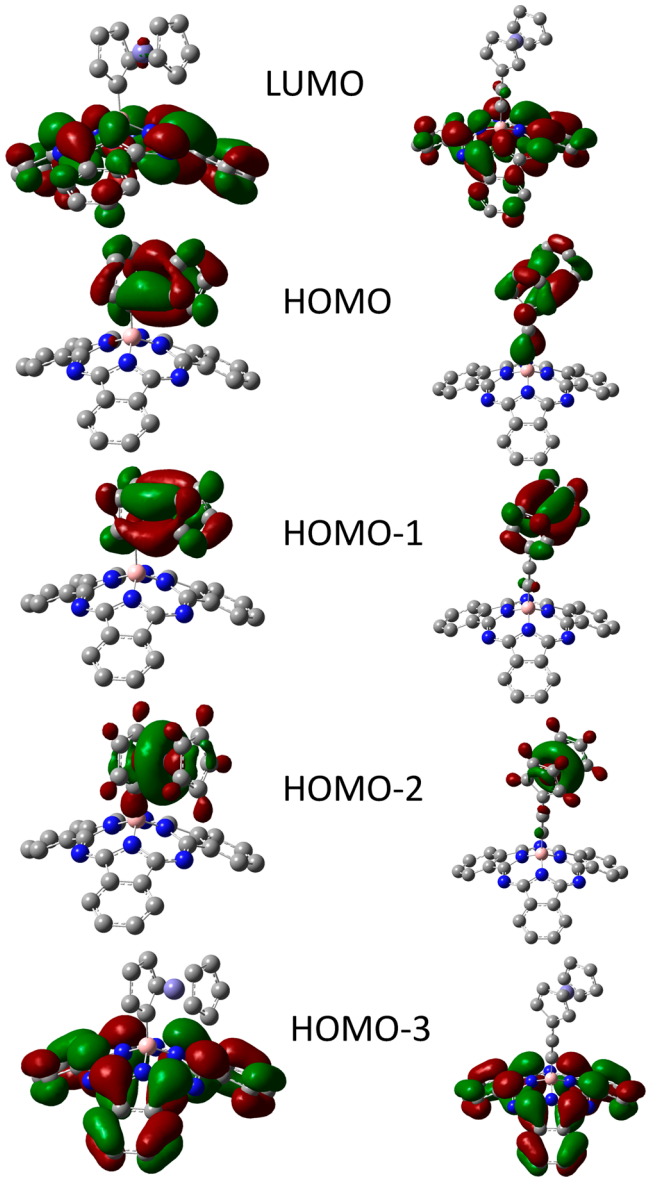

Figure 11. Frontier orbitals of compounds **2** and **3** predicted at the DFT-PCM level.

characterize the rapid excited state deactivation and subsequent recovery of the ground state via a charge transfer intermediate.

Transient difference spectra following $\pi^* \leftarrow \pi$ excitation at 560 nm for **1**−**5** are shown in Figures 5 and 6. In Figure 5, overlapping transient absorption (TA) and the ground state bleach (GSB) result in a differential shape. For **1** the transient spectrum is evident within the time resolution of our experiment (50 fs). The shape of the spectrum exhibits no change with time, and the amplitude decays very little during the 900 ps measured. This is consistent with the measured fluorescence lifetime of 3 ns for the parent SubPc **1**. We assign the TA that peaks around 610 nm (a result of interference between the TA and the GSB) to the initially excited singlet state of the SubPc.

Immediately after excitation (time delays <100 fs), the transient spectra from **2** and **3** were nearly identical to **1**, indicating the spectrum of the initially excited π^* state. However, the spectra for **2**−**5** subsequently underwent rapid evolution not found in the case of **1**. The peak in the TA shifted

dx.doi.org/10.1021/ic5014544 | Inorg. Chem. 2014, 53, 9336−9347

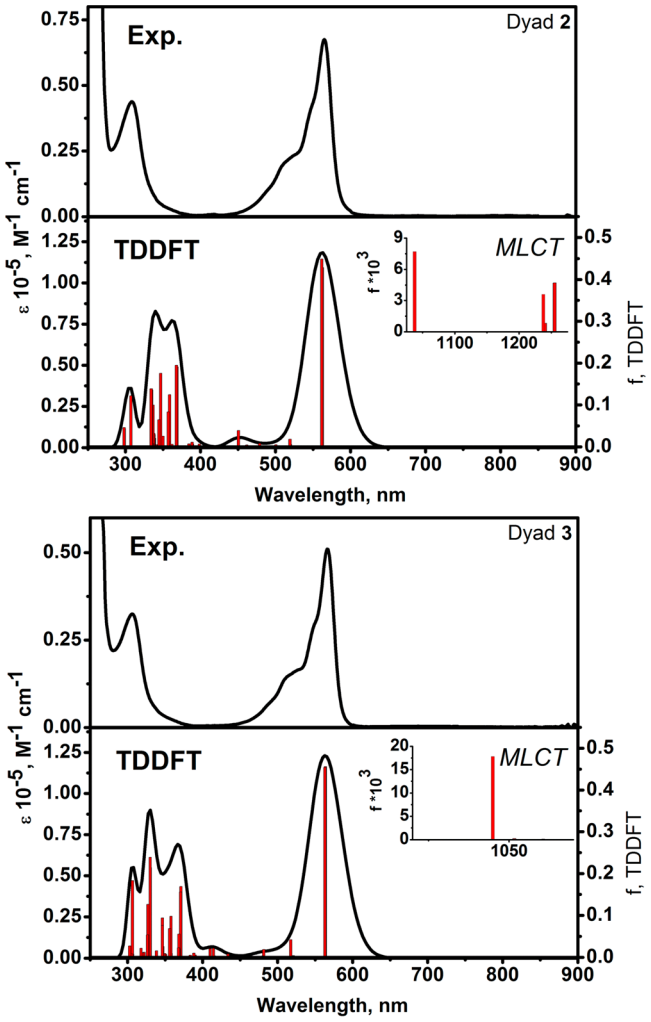

Figure 12. Experimental and predicted at TDDFT-PCM level (bottom) UV−vis spectra of dyad **2** (top) and **3** (bottom).

from 610 nm to about 570 nm in less than 10 ps. The initial shift was followed by nearly complete decay in the amplitude of both the TA and the GSB during the 900 ps probed. This indicated a return to the original ground state in less than 1 ns. The Glotaran software package was used to fit the spectra as linear combinations of individual spectral components that have time-dependent amplitudes.[34] Two primary spectral components were sufficient to represent the measured pump−probe spectra (Figure S5, Supporting Information), and these are presented in Figure 7 for **2** and **3** along with the time evolution of the amplitude of each component. The analogous figures for **4** and **5** are presented in Figure S6, Supporting Information. Exponential time constants determined from the fitting are presented in Table 3. The differential shape with TA peaked at 570 nm is consistent with absorption from the reduced SubPc.[35] On the basis of this, and the oxidative return of the fluorescence presented in the next section, we assign the observed dynamics to quenching of the excited state via electron transfer from the ferrocene substituent followed by subsequent decay of the charge transfer state:

$$\text{SubPcB-L-Fc} \xrightarrow{h\nu} \text{SubPcB*-L-Fc} \xrightarrow{\tau_{ET}} \text{SubPcB}^{-}\text{-L-Fc}^{+} \xrightarrow{\tau_{BET}} \text{SubPcB-L-Fc}$$

L = nil (**2**), −C ≡ C-(**3**), -OCH$_2$- (**4**), -O$_2$C- (**5**)

Direct axial linkage of the Fc, **2**, resulted in ultrafast, 200 fs deactivation of the excited state via reduction of the SubPc and a relatively short-lived charge transfer state with a lifetime of 41 ps. Addition of the ethynyl spacer, **3**, increased the donor−acceptor distance, slowed the forward electron transfer by an order of magnitude to 1.9 ps, and doubled the lifetime of the charge transfer state. The ether, **4**, and ester, **5**, linkages also resulted in initial charge transfer on a picosecond time scale. Transfer with the ester was about 4 times faster than with the ether. In agreement with these pump−probe measurements, previous experiments using time-resolved fluorescence determined that the quenching in **4** and **5** takes place very rapidly.[11] However, limitations on the time resolution of the fluorescence experiments prevented an accurate determination of the time constants. The distance between the Fc donor and the SubPc acceptor is very similar in **3**−**5**,[11] and the resulting forward electron transfer rates are also very similar. Quantitative agreement in the rates between **3** and **5** can be explained by the similarity in the relative orientations of the Fc and SubPc. In **4**, the axial ferrocene-containing ligand has greater conformational flexibility relative to **3** and **5**, and the rate of forward electron transfer is modestly reduced.

Although the rates of forward transfer in **3** and **5** are nearly the same, the back electron transfer for **5** is significantly slower than for **3**. The reorganization energies are expected to be very similar for this series comprised of identical donor and acceptor moieties. Slowing of the back electron transfer may reflect the greater conformational flexibility provided by the ester linkage compared with the ethynyl. That flexibility allows for larger changes in the relative orientations of the Fc and SubPc following forward charge transfer in **5**. The result could be reduced donor−acceptor electronic coupling following equilibration in the charge transfer state that slows the back electron transfer.

The transient spectroscopy experiments are indicative of the standard quenching mechanism in ferrocene-containing compounds, i.e., electron-transfer from the low-spin iron(II) center in ferrocene substituent to the photoexcited subphthalocyanine core.[7] Given such a mechanism, oxidation of the iron center should partially restore the fluorescence of the macrocycle. Figure 8 presents the measured fluorescence recovery following stepwise oxidation of the ferrocene substituents by $Fe(ClO_4)_3$ in dyads **2**−**4**. Because of the higher oxidation potential of the Fc ligand, complex **5** was titrated with a stronger oxidant, Br_2. It is interesting to note that the emission profiles for redox-activated fluorescence in dyads **4** and **5** are close to the emission spectrum of the parent compound **1**, while emission profiles of dyads **2** and **3** display different relative intensities in the observed primary vibronic progression. This difference in the Franck−Condon progression indicates different vibronic coupling to the $\pi \rightarrow \pi^*$ electronic transition in complexes **2** and **3** compared to complexes **4** and **5**.

Further insights into the redox behavior, UV−vis spectroscopy, and electronic structure of the new organoboryl complexes **2** and **3** as well as reference compounds **1**, **4**, and **5** were obtained on the basis of DFT-PCM and TDDFT-PCM calculations, which allow predictions of spectroscopy and energies of a large number of ferrocene-containing compounds[36] as well as aromatic macrocycles including SubPcs with a great accuracy.[11,16,37] The energy diagram for SubPcs **1**−**5** predicted at the DFT-PCM level is shown in Figure 9, while an analysis of the orbital compositions is provided in Figure 10. In addition, the frontier orbitals of the new SubPc complexes **2**

dx.doi.org/10.1021/ic5014544 | Inorg. Chem. 2014, 53, 9336−9347

and **3** are presented in Figure 11. The HOMO, HOMO-1, and HOMO-2 in dyads **2** and **3** were predicted to be predominantly iron (d_{xy}, $d_{x^2-y^2}$, and d_{z^2}, respectively)—centered MOs localized on the axial ferrocene fragment (Figure 11) with the first SubPc-centered occupied π-orbital being the HOMO-3, which correlates well with previous DFT calculations on dyads **4** and **5**. Such a molecular orbital description correlates well with the redox data, which suggest that the first oxidation in complexes **2** and **3** is localized at ferrocene fragment. The ferrocenyl-centered HOMO in dyad **3** is ~0.12 eV more stable than the HOMO in complex **2**. In addition, the HOMO-4 and HOMO-5 in dyad **3** have a significant contribution from the -C≡C- bridge. The LUMO and LUMO+1 in dyads **2** and **3** are π^* MOs centered on the macrocyclic core and are almost degenerate. The LUMO and LUMO+1 are well separated by energy from the LUMO+2.

In order to confirm a tentative assignment of the UV−vis spectra of dyads **2** and **3** as well as to probe possible MLCT transitions in these complexes, we have conducted TDDFT-PCM calculations. Similar to our previous report, TDDFT-PCM predicted UV−vis spectra of dyads **2** and **3** correlate well with the experimentally observed data. Predicted at the TDDFT-PCM level UV−vis spectra of **2** and **3** on the nanometer scale are shown in Figure 12 in comparison with the experimental data, while the same data on the cm^{-1} scale are shown in Supporting Information, Figure S7 (Supporting Information, Table S2 provides expansion coefficients for all transitions). The typical errors in our TDDFT-PCM calculations for dyads **2** and **3** were found to be very reasonable (~0.1−0.2 eV), which correlates well with earlier reports.[16,37,38] Similar to the previous publications on SubPcs, the Q-band region (~500−600 nm) in dyads **2** and **3** is dominated by the two intraligand subphthalocyanine $\pi \rightarrow \pi^*$ transitions, which have the HOMO-3 → LUMO and HOMO-3 → LUMO+1 origin. The B-band region (~300−350 nm) in SubPcs **2** and **3** is dominated by the number of intraligand subphthalocyanine $\pi \rightarrow \pi^*$ transitions with the HOMO-9 → LUMO and HOMO-9 → LUMO+1 being the most intense. The TDDFT-PCM calculations for organoboryl complexes **2** and **3** also predicted several MLCT transitions with the energies lower than the Q-band region (Figure 12). Specifically, TDDFT-PCM calculations predict that the MLCT region should be located at NIR region and originate from six transitions, which predominantly come from excitations from ferrocene-centered HOMO, HOMO-1, and HOMO-2 to SubPc centered LUMO and LUMO+1. According to TDDFT-PCM calculations, however, the intensities of these MLCT transitions should be much smaller that intraligand subphthalocyanine $\pi \rightarrow \pi^*$ transitions. Not surprisingly, MLCT transitions were not observed in the experimental UV−vis spectra of new dyads **2** and **3**. In general, TDDFT-PCM predicted UV−vis spectra of new dyads **2** and **3** are in excellent agreement with the experimental data on these compounds and suggestive of the $\pi \rightarrow \pi^*$ transitions dominance in both Q- and B-band regions.

CONCLUSIONS

Two new organoboryl ferrocenyl-subphthalocyanine complexes with ferrocene (**2**) and ethynylferrocene (**3**) fragments directly bonded to the boron atom using a B−C bond have been prepared using reaction between SubPcBCl and FcLi (**2**) or FcC≡CMgBr (**3**). Target compounds were characterized by spectroscopic (UV−vis, NMR, and MCD) and X-ray crystallography methods. Trigonal pyramidal (3N+C) coordination of the boron center in complexes **2** and **3** was confirmed by the X-ray crystallography. Redox potentials of organoboryl complexes **2** and **3** were studied by CV and DPV approaches in DCM/0.1 M TBAP and DMF/0.1 M TBAP systems and correlated to those in subphthalocyanine **1** as well as reported earlier dyads **4** and **5**. The first oxidation in dyads **2** and **3** was found to be reversible and centered at the ferrocene fragment, respectively. The first reduction and the second oxidation were found to be centered at the subphthalocyanine core. DFT-PCM and TDDFT-PCM calculations were used to elucidate the electronic structures in new dyads **2** and **3** and to support a tentative assignment of the intense bands observed in the UV−vis spectra of complexes **2** and **3**. DFT-PCM approach predicts that the HOMO, HOMO-1, and HOMO-2 in complexes **2** and **3** should be centered at the ferrocene group, while HOMO-3 as well as LUMO and LUMO+1 should be π or π^* MOs in nature and centered at the subphthalocyanine core. The vertical excitation energies in complexes **2** and **3** were predicted by the TDDFT-PCM method and correlate well with the experimental UV−vis spectra. On the basis of the predicted oscillator strengths, it was suggested that the $\pi \rightarrow \pi^*$ transitions should dominate in their UV−vis spectra. Although the TDDFT-PCM calculations predict several MLCT transitions in the NIR region for complexes **2** and **3**, their intensities are rather weak, and these bands were not observed in experiments. The steady-state, time-resolved, and oxidative titration fluorescence data were collected for subphthalocyanines **1**−**5**. The results demonstrate that the excited state quenching takes place via electron transfer from the ferrocene to the SubPc, and subsequent back electron transfer to the original ground state occurs in less than 1 ns. Comparison between the dyads indicates that the dominant coupling between donor and acceptor is through space and controlled by distance and orientation. Additional conformational flexibility in the ether and ester bridges compared with the ethynyl bridge allows for additional reorientation in the charge separated state that slows charge recombination by a factor of about 4.

ASSOCIATED CONTENT

Supporting Information

Crystallographic data for complexes **2** and **3** in CIF format. Coordinates for DFT-PCM optimized structures of **2** and **3**. Predicted by TDDFT-PCM expansion coefficients for dyads **2** and **3**. Predicted by TDDFT-PCM and experimental and UV−vis spectra of dyads **2** and **3** in cm^{-1} scale. This material is available free of charge via the Internet at http://pubs.acs.org.

AUTHOR INFORMATION

Corresponding Authors

*(V.N.N.) E-mail: vnemykin@d.umn.edu.
*(D.A.B.) E-mail: blank@umn.edu.

Notes

The authors declare no competing financial interest.

ACKNOWLEDGMENTS

Generous support from the NSF CHE-1110455, CHE-1401375, and NSF MRI CHE-0922366, Minnesota Supercomputing Institute, and U of M Grant-in-Aid to V.N. is greatly appreciated. D.A.B. gratefully acknowledges support of this work by NSF under Grant DMR-1006566. The authors thank Alexander Gulachek for his help with the fluorescence quantum yield measurements.

REFERENCES

(1) (a) Sun, Y.; Welch, G. C.; Leong, W. L.; Takacs, C. J.; Bazan, G. C.; Heeger, A. J. *Nat. Mater.* **2012**, *11*, 44−48. (b) Whittell, G. R.; Hager, M. D.; Schubert, U. S.; Manners, I. *Nat. Mater.* **2011**, *10*, 176−188. (c) *Electron Transfer in Chemistry*; Balzani, V., Ed.; Wiley-VCH: Weinheim, Germany, 2001; Vols. *I*−*V*. (d) Melkozernov, A. N.; Barber, J.; Blankenship, R. E. *Biochemistry* **2006**, *45*, 331−345. (e) Guenes, S.; Neugebauer, H.; Sariciftci, N. S. *Chem. Rev.* **2007**, *107*, 1324−1338.

(2) (a) Imahori, H.; Mori, Y.; Matano, Y. *J. Photochem. Photobiol. C* **2003**, *4*, 51−83. (b) Imahori, H.; Tamaki, K.; Araki, Y.; Sekiguchi, Y.; Ito, O.; Sakata, Y.; Fukuzumi, S. *J. Am. Chem. Soc.* **2002**, *124*, 5165−5174. (c) D'Souza, F.; Chitta, R.; Gadde, S.; Islam, D.-M. S.; Schumacher, A. L.; Zandler, M. E.; Araki, Y.; Ito, O. *J. Phys. Chem. B* **2006**, *110*, 25240−25250. (d) Springer, J.; Kodis, G.; De La Garza, L.; Moore, A. L.; Moore, T. A.; Gust, D. *J. Phys. Chem. A* **2003**, *107*, 3567−3575. (e) González-Rodríguez, D.; Bottari, G. *J. Porphyrins Phthalocyanines* **2009**, *13*, 624−636.

(3) *Molecular Mechanisms of Photosynthesis*; Blankenship, R. E., Ed.; Blackwell Science: Malden, MA, 2002.

(4) (a) Aratani, N.; Osuka, A. In *Handbook of Porphyrin Science*; Kadish, K. M., Smith, K. M., Guilard, R., Eds.; World Scientific Publishing Co. Pte. Ltd.: Singapore, 2010; Vol. *1*, pp 1 − 132. (b) Balaban, T. S. in: *Handbook of Porphyrin Science*. Kadish, K. M.; Smith, K. M.; Guilard, R. (Eds.); World Scientific Publishing Co. Pte. Ltd. 2010, Vol. *1*, pp 221−306. (c) Zhao, Z.; Cammidge, A. N.; Cook, M. J. *Chem. Commun.* **2009**, 7530−7532.

(5) (a) Yoon, Z. S.; Yang, J.; Yoo, H.; Cho, S.; Kim, D. In *Handbook of Porphyrin Science*; Kadish, K. M., Smith, K. M., Guilard, R., Eds.; World Scientific Publishing Co. Pte. Ltd.: Singapore, 2010; Vol. *1*, pp 439−506. (b) Gonzalez-Rodriguez, D.; Carbonell, E.; Rojas, G. M.; Castellanos, C. A.; Guldi, D. M.; Torres, T. *J. Am. Chem. Soc.* **2010**, *132*, 16488−16500. (c) El-Khouly, M. E.; Shim, S. H.; Araki, Y.; Ito, O.; Kay, K.-Y. *J. Phys. Chem. B* **2008**, *112*, 3910−3917. (d) Solntsev, P. V.; Sabin, J. R.; Dammer, S. J.; Gerasimchuk, N. N.; Nemykin, V. N. *Chem. Commun.* **2010**, 6581−6583. (e) Ziessel, R.; Ulrich, G.; Elliott, K. J.; Harriman, A. *Chem.—Eur. J.* **2009**, *15*, 4980−4984. (f) Mauldin, C. E.; Piliego, C.; Poulsen, D.; Unruh, D. A.; Woo, C.; Ma, B.; Mynar, J. L.; Frechet, J. M. J. *ACS Appl. Mater. Interfaces* **2010**, *2*, 2833−2838. (g) Gonzalez-Rodriguez, D.; Torres, T.; Olmstead, M. M.; Rivera, J.; Angeles Herranz, M.; Echegoyen, L.; Atienza Castellanos, C.; Guldi, D. M. *J. Am. Chem. Soc.* **2006**, *128*, 10680−10681.

(6) (a) Grimm, B.; Hausmann, A.; Kahnt, A.; Seitz, W.; Spanig, F.; Guldi, D. M. In *Handbook of Porphyrin Science*; Kadish, K. M., Smith, K. M., Guilard, R., Eds.; World Scientific Publishing Co. Pte. Ltd.: Singapore, 2010; Vol. *1*, pp 133− 220. (b) Araki, Y.; Ito, O. *J. Photochem. Photobiol. C* **2008**, *9*, 93−110. (c) Guldi, D. M.; Hirsch, A.; Scheloske, M.; Dietel, E.; Troisi, A.; Zerbetto, F.; Prato, M. *Chem.—Eur. J.* **2003**, *9*, 4968−4979. (d) Albinsson, B.; Eng, M. P.; Pettersson, K.; Winters, M. U. *Phys. Chem. Chem. Phys.* **2007**, *9*, 5847−5864. (e) Nieto, C. R.; Guilleme, J.; Villegas, C.; Delgado, J. L.; Gonzalez-Rodriguez, D.; Martin, N.; Torres, T.; Guldi, D. M. *J. Mater. Chem.* **2011**, *21*, 15914−15918. (f) Rohde, G. T.; Sabin, J. R.; Barrett, C. D.; Nemykin, V. N. *New J. Chem.* **2011**, *35*, 1440−1448. (g) Nemykin, V. N.; Rohde, G. T.; Barrett, C. D.; Hadt, R. G.; Sabin, J. R.; Reina, G.; Galloni, P.; Floris, B. *Inorg. Chem.* **2010**, *49*, 7497−7509. (h) Nemykin, V. N.; Rohde, G. T.; Barrett, C. D.; Hadt, R. G.; Bizzarri, C.; Galloni, P.; Floris, B.; Nowik, I.; Herber, R. H.; Marrani, A. G.; Zanoni, R.; Loim, N. M. *J. Am. Chem. Soc.* **2009**, *131*, 14969−14978. (i) Nemykin, V. N.; Galloni, P.; Floris, B.; Barrett, C. D.; Hadt, R. G.; Subbotin, R. I.; Marrani, A. G.; Zanoni, R.; Loim, N. M. *Dalton Trans.* **2008**, 4233−4246. (j) Nemykin, V. N.; Barrett, C. D.; Hadt, R. G.; Subbotin, R. I.; Maximov, A. Y.; Polshin, E. V.; Koposov, A. Y. *Dalton Trans.* **2007**, 3378−3389. (k) Vecchi, A.; Gatto, E.; Floris, B.; Conte, V.; Venanzi, M.; Nemykin, V. N.; Galloni, P. *Chem. Commun.* **2012**, *48*, 5145−5147. (l) Nemykin, V. N.; Purchel, A. A.; Spaeth, A. D.; Barybin, M. V. *Inorg. Chem.* **2013**, *52*, 11004−11012. (m) Dammer, S. J.; Solntsev, P. V.; Sabin, J. R.; Nemykin, V. N. *Inorg. Chem.* **2013**, *52*, 9496−9510. (n) Vecchi, A.; Galloni, P.; Floris, B.; Nemykin, V. N. *J. Porphyrins Phthalocyanines* **2013**, *17*, 165−196. (o) Sirbu, D.; Turta, C.; Benniston, A. C.; Abou-Chahine, F.; Lemmetyinen, H.; Tkachenko, N. V.; Wood, C.; Gibson, E. *RSC Adv.* **2014**, *4*, 22733−22742.

(7) (a) D'Souza, F.; Ito, O. In *Handbook of Porphyrin Science*; Kadish, K. M., Smith, K. M., Guilard, R., Eds.; World Scientific Publishing Co. Pte. Ltd.: Singapore, 2010; Vol. *1*, pp 307−438. (b) El-Khouly, M. E.; Ito, O.; Smith, P. M.; D'Souza, F. *J. Photochem. Photobiol., C* **2004**, *5*, 79−104. (c) Fukuzumi, S. *Phys. Chem. Chem. Phys.* **2008**, *10*, 2283−2297. (d) D'Souza, F.; Ito, O. *Organic Electronics and Photonics*; Nalwa, H. R., Ed.; American Scientific Publishers: Stevenson Ranch, CA, 2008; Vol. *1*, Chapter 13. (e) Ohkubo, K.; Fukuzumi, S. *Bull. Chem. Soc. Jpn.* **2009**, *82*, 303−315.

(8) Ohkubo, K.; Kotani, H.; Shao, J.; Ou, Z.; Kadish, K. M.; Li, G.; Pandey, R. K.; Fujitsuka, M.; Ito, O.; Imahori, H.; Fukuzumi, S. *Angew. Chem., Int. Ed.* **2004**, *43*, 853−856.

(9) (a) Verreet, B.; Rand, B. P.; Cheyns, D.; Hadipour, A.; Aernouts, T.; Heremans, P.; Medina, A.; Claessens, C. G.; Torres, T. *Adv. Energy Mater.* **2011**, *1*, 565−568. (b) Luhman, W. A.; Holmes, R. J. *Adv. Funct. Mater.* **2011**, *21*, 764−771. (c) Shimizu, S.; Nakano, S.; Hosoya, T.; Kobayashi, N. *Chem. Commun.* **2011**, *47*, 316−318. (d) Gonzalez-Rodriguez, D.; Carbonell, E.; Guldi, D. M.; Torres, T. *Angew. Chem., Int. Ed.* **2009**, *48*, 8032−8036. (e) Verreet, B.; Schols, S.; Cheyns, D.; Rand, B. P.; Gommans, H.; Aernouts, T.; Heremans, P.; Genoe, J. *J. Mater. Chem.* **2009**, *19*, 5295−5297. (f) Gonzalez-Rodriguez, D.; Torres, T.; Herranz, M. A.; Echegoyen, L.; Carbonell, E.; Guldi, D. M. *Chem.—Eur. J.* **2008**, *14*, 7670−7679. (g) Kim, J.-H.; El-Khouly, M. E.; Araki, Y.; Ito, O.; Kay, K.-Y. *Chem. Lett.* **2008**, *37*, 544−545. (h) Iglesias, R. S.; Claessens, C. G.; Rahman, G. M. A.; Herranz, M. A.; Guldi, D. M.; Torres, T. *Tetrahedron* **2007**, *63*, 12396−12404. (i) Claessens, C. G.; Gonzalez-Rodriguez, D.; Iglesias, R. S.; Torres, T. *C. R. Chimie* **2006**, *9*, 1094−1099. (j) Claessens, C. G.; Torres, T. *Chem. Commun.* **2004**, 1298−1299. (k) Gonzalez-Rodriguez, D.; Torres, T.; Guldi, D. M.; Rivera, J.; Herranz, M. A.; Echegoyen, L. *J. Am. Chem. Soc.* **2004**, *126*, 6301−6313.

(10) (a) Wrobel, D.; Boguta, A.; Mazurkiewicz, P. *Spectrochim. Acta. A* **2003**, *59*, 2841−54. (b) Kobayashi, N. *J. Chem. Soc., Chem. Commun.* **1991**, 1203−1205. (c) Yanagi, H.; Mukai, H.; Nair, M. *Thin Solid Films* **2006**, *499*, 123−128. (d) Xu, S.; Chen, K.; Tian, H. *J. Mater. Chem.* **2005**, *15*, 2676−2680. (e) Gonzalez-Rodriguez, D.; Claessens, C. G.; Torres, T.; Liu, S.; Echegoyen, L.; Vila, N.; Nonell, S. *Chem.—Eur. J.* **2005**, *11*, 3881−3893. (f) Ohno-Okumura, E.; Sakamoto, K.; Kato, T.; Hatano, T.; Fukui, K.; Karatsu, T.; Kitamura, A.; Urano, T. *Dyes Pigments* **2002**, *53*, 57−65. (g) Rahman, G. M. A.; Lueders, D.; Rodriguez-Morgade, M. S.; Caballero, E.; Torres, T.; Guldi, D. M. *ChemSusChem* **2009**, *2*, 330−335. (h) Xu, H.; Ng, D. K. P. *Chem.—Asian J.* **2009**, *4*, 104−110. (i) Diaz, D. D.; Bolink, H. J.; Cappelli, L.; Claessens, C. G.; Coronado, E.; Torres, T. *Tetrahedron Lett.* **2007**, *48*, 4657−4660. (j) Geyer, M.; Plenzig, F.; Rauschnabel, J.; Hanack, M.; Del Rey, B.; Sastre, A.; Torres, T. *Synthesis* **1996**, 1139−1151. (k) Medina, A.; Claessens, C. G.; Rahman, G. M. A.; Lamsabhi, A. M.; Mo, O.; Yanez, M.; Guldi, D. M.; Torres, T. *Chem. Commun.* **2008**, 1759−1761. (l) Xu, H.; Jiang, X.-J.; Chan, E. Y. M.; Fong, W.-P.; Ng, D. K. P. *Org. Biomol. Chem.* **2007**, *5*, 3987−3992.

(11) Solntsev, P. V.; Spurgin, K. L.; Sabin, J. R.; Heikal, A. A.; Nemykin, V. N. *Inorg. Chem.* **2012**, *51*, 6537−6547.

(12) (a) Adamo, C.; Barone, V. *J. Chem. Phys.* **1999**, *110*, 6158−6169. (b) Perdew, J. P.; Burke, K.; Ernzerhof, M. *Phys. Rev. Lett.* **1996**, *77*, 3865−3868. (c) Perdew, J. P.; Burke, K.; Ernzerhof, M. *Phys. Rev. Lett.* **1997**, *78*, 1396−1396.

(13) (a) Firme, C. L.; Pontes, D. de L.; Antunes, O. A. C. *Chem. Phys. Lett.* **2010**, *499*, 193−198. (b) Kalamse, V.; Wadnerkar, N.; Chaudhari, A. *J. Phys. Chem. C* **2010**, *114*, 4704−4709. (c) Meylemans, H. A.; Damrauer, N. H. *Inorg. Chem.* **2009**, *48*, 11161−11175. (d) Alparone, A.; Reis, H.; Papadopoulos, M. G. *J. Phys. Chem. A* **2006**, *110*, 5909−5918. (e) Solntsev, P. V.; Dudkin, S. V.; Sabin, J. R.; Nemykin, V. N. *Organometallics* **2011**, *30*, 3037−3046. (f) Goetsch, W. R.; Solntsev, P. V.; Van Stappen, C.; Purchel, A. A.; Dudkin, S. V.; Nemykin, V. N. *Organometallics* **2014**, *33*, 145−157.

(14) Tomasi, J.; Mennucci, B.; Cammi, R. *Chem. Rev.* **2005**, *105*, 2999−3093.
(15) (a) Becke, A. D. *Phys. Rev. A* **1988**, *38*, 3098−3100. (b) Perdew, J. P. *Phys. Rev. B* **1986**, *33*, 8822−8824.
(16) (a) Nemykin, V. N.; Hadt, R. G. *J. Phys. Chem. A* **2010**, *114*, 12062−12066. (b) Nemykin, V. N.; Hadt, R. G.; Belosludov, R. V.; Mizuseki, H.; Kawazoe, Y. *J. Phys. Chem. A* **2007**, *111*, 12901−12913. (c) Zhang, L.; Qi, D.; Zhang, Y.; Bian, Y.; Jiang, J. *J. Mol. Graph. Model.* **2011**, *29*, 717−725. (d) Zarate, X.; Schott, E.; Arratia-Perez, R. *Int. J. Quantum Chem.* **2011**, *111*, 4186−4196. (e) Soldatova, A. V.; Kim, J.-H.; Rizzoli, C.; Kenney, M. E.; Rodgers, M. A. J.; Rosa, A.; Ricciardi, G. *Inorg. Chem.* **2011**, *50*, 1135−1149. (f) Ricciardi, G.; Soldatova, A. V.; Rosa, A. *J. Porphyrins Phthalocyanines* **2010**, *14*, 689−700. (g) Sabin, J. R.; Varzatskii, O. A.; Voloshin, Y. Z.; Starikova, Z. A.; Novikov, V. V.; Nemykin, V. N. *Inorg. Chem.* **2012**, *51*, 8362−8372.
(17) Wachters, A. J. H. *J. Chem. Phys.* **1970**, *52*, 1033−1036.
(18) McLean, A. D.; Chandler, G. S. *J. Chem. Phys.* **1980**, *72*, 5639−5648.
(19) Frisch, M. J.; Trucks, G. W.; Schlegel, H. B.; Scuseria, G. E.; Robb, M. A.; Cheeseman, J. R.; Scalmani, G.; Barone, V.; Mennucci, B.; Petersson, G. A.; Nakatsuji, H.; Caricato, M.; Li, X.; Hratchian, H. P.; Izmaylov, A. F.; Bloino, J.; Zheng, G.; Sonnenberg, J. L.; Hada, M.; Ehara, M.; Toyota, K.; Fukuda, R.; Hasegawa, J.; Ishida, M.; Nakajima, T.; Honda, Y.; Kitao, O.; Nakai, H.; Vreven, T.; Montgomery, Jr., J. A.; Peralta, J. E.; Ogliaro, F.; Bearpark, M.; Heyd, J. J.; Brothers, E.; Kudin, K. N.; Staroverov, V. N.; Kobayashi, R.; Normand, J.; Raghavachari, K.; Rendell, A.; Burant, J. C.; Iyengar, S. S.; Tomasi, J.; Cossi, M.; Rega, N.; Millam, N. J.; Klene, M.; Knox, J. E.; Cross, J. B.; Bakken, V.; Adamo, C.; Jaramillo, J.; Gomperts, R.; Stratmann, R. E.; Yazyev, O.; Austin, A. J.; Cammi, R.; Pomelli, C.; Ochterski, J. W.; Martin, R. L.; Morokuma, K.; Zakrzewski, V. G.; Voth, G. A.; Salvador, P.; Dannenberg, J. J.; Dapprich, S.; Daniels, A. D.; Farkas, Ö.; Foresman, J. B.; Ortiz, J. V.; Cioslowski, J.; Fox, D. J. *Gaussian 09*, Revision A.1; Gaussian, Inc.: Wallingford, CT, 2009.
(20) Tenderholt, A. L. *QMForge*, Version 2.1; Stanford University, Stanford, CA, USA.
(21) Otwinowski, Z.; Minor, W. *Methods in Enzymology*; Carter Jr, C. W.; Sweet, R. M., Eds.; Academic Press: New York, 1997; Vol. *276*, pp 307—326.
(22) Altomare, A.; Cascarano, G.; Giacovazzo, C.; Guagliardi, A.; Burla, M. C.; Polidori, G.; Camalli, M. *J. Appl. Crystallogr.* **1994**, *27*, 435.
(23) Sheldrick, G. M. *Acta Crystallogr.* **2008**, *A64*, 112−122.
(24) Malessa, M.; Heck, J.; Kopf, J.; Garcia, M. H. *Eur. J. Inorg. Chem.* **2006**, 857−867.
(25) Stepnicka, P.; Podlaha, J.; Horacek, M.; Hanus, V.; Mach, K. *J. Organomet. Chem.* **1999**, *580*, 210−213.
(26) (a) Del Rey, B.; Keller, U.; Torres, T.; Rojo, G.; Agullo-Lopez, F.; Nonell, S.; Marti, C.; Brasselet, S.; Ledoux, I.; Zyss, J. *J. Am. Chem. Soc.* **1998**, *120*, 12808−12817. (b) Kasuga, K.; Idehara, T.; Handa, M.; Ueda, Y.; Fujiwara, T.; Isa, K. *Bull. Chem. Soc. Jpn.* **1996**, *69*, 2559−2563. (c) Gonzalez-Rodriguez, D.; Torres, T.; Denardin, E. L. G.; Samios, D.; Stefani, V.; Correa, D. S. *J. Organomet. Chem.* **2009**, *694*, 1617−1622. (d) Morse, G. E.; Paton, A. S.; Lough, A.; Bender, T. P. *Dalton Trans.* **2010**, 3915−3922. (e) Lapok, L.; Claessens, C. G.; Woehrle, D.; Torres, T. *Tetrahedron Lett.* **2009**, *50*, 2041−2044. (f) Claessens, C. G.; Gonzalez-Rodriguez, D.; del Rey, B.; Torres, T.; Mark, G.; Schuchmann, H.-P.; von Sonntag, C.; MacDonald, J. G.; Nohr, R. S. *Eur. J. Org. Chem.* **2003**, 2547−2551.
(27) Guilleme, J.; Gonzalez-Rodriguez, D.; Torres, T. *Angew. Chem., Int. Ed.* **2011**, *50*, 3506−3509.
(28) Potz, R.; Goldner, M.; Huckstadt, H.; Cornelissen, U.; Tutass, A.; Homborg, H. *Z. Anorg. Allg. Chem.* **2000**, *626*, 588−596.
(29) (a) Engel, M. K.; Yao, J.; Maki, H.; Takeuchi, H.; Yonehara, H.; Pac, C. *Rep. Kawamura Inst. Chem. Res.* **1997**, *9*, 53−128. (b) Tippmann, E. M.; Schultz, P. G. *Tetrahedron* **2007**, *63*, 6182−6184. (c) Kato, T.; Tham, F. S.; Boyd, P. D. W.; Reed, C. A. *Heteroatom Chem.* **2006**, *17*, 209−216.
(30) Camerel, F.; Ulrich, G.; Retailleau, P.; Ziessel, R. *Angew. Chem., Int. .Ed.* **2008**, *47*, 8876−8880.
(31) (a) Ona-Burgos, P.; Casimiro, M.; Fernandez, I.; Navarro, A. V.; Fernandez Sanchez, J. F.; Carretero, A. S.; Gutierrez, A. F. *Dalton Trans.* **2010**, *39*, 6231−6238. (b) Koyama, T.; Suzuki, T.; Hanabusa, K.; Shirai, H.; Kobayashi, N. *Inorg. Chim. Acta* **1994**, *218*, 41−45. (c) Abraham, R. J.; Medforth, C. J. *Magn. Reson. Chem.* **1988**, *26*, 803−812. (d) Nemykin, V. N.; Kobayashi, N.; Chernii, V. Y.; Belsky, V. K. *Eur. J. Inorg. Chem.* **2001**, 733−743. (e) Nemykin, V. N.; Polshina, A. E.; Chernii, V. Y.; Polshin, E. V.; Kobayashi, N. *Dalton Trans.* **2000**, 1019−1025.
(32) (a) Claessens, C. G.; Gonzalez-Rodriguez, D.; Torres, T. *Chem. Rev.* **2002**, *102*, 835−853. (b) Kobayashi, N. In *The Porphyrin Handbook*; Kadish, K. M., Smith, K. M., Guilard, R., Eds.; Academic Press: New York, 2003; Vol *15*, pp 161−262.
(33) (a) Gonzalez-Rodriguez, D.; Martinez-Diaz, M. V.; Abel, J.; Perl, A.; Huskens, J.; Echegoyen, L.; Torres, T. *Org. Lett.* **2010**, *12*, 2970−2973. (b) Sakamoto, K.; Ohno-Okumura, E. *Materials* **2009**, *2*, 1127−1179. (c) Camerel, F.; Ulrich, G.; Retailleau, P.; Ziessel, R. *Angew. Chem., Int. Ed.* **2008**, *47*, 8876−8880. (d) Iglesias, R. S.; Claessens, C. G.; Herranz, M. A.; Torres, T. *Org. Lett.* **2007**, *9*, 5381−5384. (e) Iglesias, R. S.; Claessens, C. G.; Torres, T.; Herranz, M. A.; Ferro, V. R.; Garcia de la Vega, J. M. *J. Org. Chem.* **2007**, *72*, 2967−2977.
(34) Snellenburg, J. J.; Laptenok, S. P.; Seger, R.; Mullen, K. M. *J. Stat. Soft.* **2012**, *49*, 1−22.
(35) (a) El-Khouly, M. E.; Fukuzumi, S. *J. Porphyrins Phthalocyanines* **2011**, *15*, 111−117. (b) Rahman, G. M. A.; Lueders, D.; Rodriguez-Morgade, M. S.; Caballero, E.; Torres, T.; Guldi, D. M. *ChemSusChem* **2009**, *2*, 330−335.
(36) (a) Galangau, O.; Dumas-Verdes, C.; Schmidt, E. Y.; Trofimov, B. A.; Clavier, G. *Organometallics* **2011**, *30*, 6476−6481. (b) Herber, R. H.; Nowik, I.; Grosland, J. O.; Hadt, R. G.; Nemykin, V. N. *J. Organomet. Chem.* **2008**, *693*, 1850−1856. (c) Nemykin, V. N.; Makarova, E. A.; Grosland, J. O.; Hadt, R. G.; Koposov, A. Y. *Inorg. Chem.* **2007**, *46*, 9591−9601. (d) Nemykin, V. N.; Maximov, A. Y.; Koposov, A. Y. *Organometallics* **2007**, *26*, 3138−3148. (e) Nemykin, V. N.; Hadt, R. G. *Inorg. Chem.* **2006**, *45*, 8297−8307. (f) Li, Y. L.; Han, L.; Mei, Y.; Zhang, J. Z. H. *Chem. Phys. Lett.* **2009**, *482*, 217−222. (g) Fabrizi de Biani, F.; Manca, G.; Marchetti, L.; Leoni, P.; Bruzzone, S.; Guidotti, C.; Atrei, A.; Albinati, A.; Rizzato, S. *Inorg. Chem.* **2009**, *48*, 10126−10137. (h) Li, F.; Sa, R.; Wu, K. *Mol. Phys.* **2008**, *106*, 2537−2544. (i) Santi, S.; Orian, L.; Donoli, A.; Durante, C.; Bisello, A.; Ganis, P.; Ceccon, A.; Crociani, L.; Benetollo, F. *Organometallics* **2007**, *26*, 5867−5879. (j) Zhang, W.-W.; Yu, Y.-G.; Lu, Z.-D.; Mao, W.-L.; Li, Y.-Z.; Meng, Q.-J. *Organometallics* **2007**, *26*, 865−873. (k) Parac, M.; Grimme, S. *J. Phys. Chem. A* **2002**, *106*, 6844−6850.
(37) (a) Lamsabhi, A. M.; Yanez, M.; Mo, O.; Trujillo, C.; Blanco, F.; Alkorta, I.; Elguero, J.; Caballero, E.; Rodriguez-Morgade, M. S.; Claessens, C. G.; Torres, T. *J. Porphyrins Phthalocyanines* **2011**, *15*, 1220−1230. (b) Xue, Z. L.; Mack, J.; Lu, H.; Zhang, L.; You, X. Z.; Kuzuhara, D.; Stillman, M.; Yamada, H.; Yamauchi, S.; Kobayashi, N. *Chem.—Eur. J.* **2011**, *17*, 4396−4407. (c) Jakubikova, E.; Campbell, I. H.; Martin, R. L. *J. Phys. Chem. A* **2011**, *115*, 9265−9272. (d) Zhong, A.; Zhang, Y.; Bian, Y. *J. Mol. Graph. Model.* **2010**, *29*, 470−480. (e) Mack, J.; Kobayashi, N.; Stillman, M. J. *J. Inorg. Biochem.* **2010**, *104*, 310−317. (f) Quartarolo, A. D.; Lanzo, I.; Sicilia, E.; Russo, N. *Phys. Chem. Chem. Phys.* **2009**, *11*, 4586−4592. (g) Eriksson, E. S. E.; Eriksson, L. A. *Phys. Chem. Chem. Phys.* **2011**, *13*, 7207−7217. (h) Galinato, M. G. I.; Spolitak, T.; Ballou, D. P.; Lehnert, N. *Biochemistry* **2011**, *50*, 1053−1069. (i) Uoyama, H.; Kim, K. S.; Kuroki, K.; Shin, J.-Y.; Nagata, T.; Okujima, T.; Yamada, H.; Ono, N.; Kim, D.; Uno, H. *Chem.—Eur. J.* **2010**, *16*, 4063−4074.
(38) (a) Tokura, S.; Sato, T.; Tsuneda, T.; Nakajima, T.; Hirao, K. *J. Comput. Chem.* **2008**, *29*, 1187−1197. (b) Chiba, M.; Fedorov, D. G.; Kitaura, K. *J. Chem. Phys.* **2007**, *127*, 104108−104118. (c) Seth, M.; Ziegler, T. *J. Chem. Phys.* **2006**, *124*, 144105−1441016. (d) Tawada, Y.; Tsuneda, T.; Yanagisawa, S.; Yanai, T.; Hirao, K. *J. Chem. Phys.* **2004**, *120*, 8425−8433. (e) Hirata, S.; Zhan, C.-G.; Apra, E.; Windus, T. L.; Dixon, D. A. *J. Phys. Chem. A* **2003**, *107*, 10154−10158.